SSVEP Enhancement in Mixed Reality Environment for Brain–Computer Interfaces

Jieyu Wu, Feng He, Xiaolin Xiao, *Member, IEEE*, Runyuan Gao, Lin Meng, *Member, IEEE*, Xiuyun Liu, *Senior Member, IEEE*, Minpeng Xu, *Senior Member, IEEE*, and Dong Ming, *Senior Member, IEEE*

***Abstract*— Expanding the application possibilities of brain-computer interfaces (BCIs) is possible through their implementation in mixed reality (MR) environments. However, visual stimuli are displayed against a realistic scene in the MR environment, which degrades BCI performance. The purpose of this study was to optimize stimulus colors in order to improve the MR-BCI system's performance. In the MR environment, a 10-command SSVEP-BCI was deployed. Various stimulus colors and background colors for the BCI system were tested and optimized in offline and online experiments. Color contrast ratios (CCRs) between stimulus and background colors were introduced to assess the performance difference among all conditions. Additionally, we proposed a cross-correlation task-related component analysis based on simulated annealing (SA-xTRCA), which can increase the signal-to-noise ratio (SNR) and detection accuracy by aligning SSVEP trials. The results of an offline experiment showed that the background and stimulus colors had a significant interaction effect that can impact system performance. A possible nonlinear relationship between CCR value and SSVEP detection accuracy exists. Online experiment results demonstrated that the system performed best with polychromatic stimulus on the colored background. The proposed SA-xTRCA significantly outperformed the other four traditional algorithms. The online average information transfer rate (ITR) achieved 57.58 ± 5.31 bits/min. This study proved that system performance can be effectively enhanced by optimizing stimulus color based on background color. In MR environments, CCR can be used as a quantitative criterion for choosing stimulus colors in BCI system design.**

***Index Terms*— Brain–computer interface (BCI), mixed reality (MR), stimulus color, latency calibration.**

Received 12 September 2024; revised 2 December 2024 and 3 January 2025; accepted 5 January 2025. Date of publication 8 January 2025; date of current version 17 January 2025. This work was supported in part by the National Key Research and Development Program of China under Grant 2022YFF1202500 and Grant 2022YFF1202501; and in part by the National Natural Science Foundation of China under Grant 62106170, Grant 62122059, and Grant 81925020. *(Corresponding authors: Xiaolin Xiao; Minpeng Xu.)*

This work involved human subjects or animals in its research. Approval of all ethical and experimental procedures and protocols was granted by the Research Ethics Committee of Tianjin University under Application No. TJUE-2021-046.

Jieyu Wu is with the Academy of Medical Engineering and Translational Medicine, Tianjin University, Tianjin 300072, China.

Feng He, Xiaolin Xiao, Lin Meng, Xiuyun Liu, Minpeng Xu, and Dong Ming are with the Academy of Medical Engineering and Translational Medicine, Tianjin University, Tianjin 300072, China, and also with the Haihe Laboratory of Brain-Computer Interaction and Human-Machine Integration, Tianjin 300392, China (e-mail: xiaoxiao0@tju.edu.cn; xmp52637@tju.edu.cn).

Runyuan Gao is with the Department of Biomedical Engineering, College of Precision Instruments and Optoelectronics Engineering, Tianjin University, Tianjin 300072, China.

This article has supplementary downloadable material available at https://doi.org/10.1109/TNSRE.2025.3526950, provided by the authors.

Digital Object Identifier 10.1109/TNSRE.2025.3526950

I. Introduction

ELECTROENCEPHALOGRAPHY (EEG) -based Brain-Computer Interfaces (BCIs) provide a non-invasive method of capturing brain activity signals and converting them into commands to operate external devices [1], [2], [3]. Numerous intent-related electrophysiological features [4], [5], [6] have been discovered and employed in BCI systems [7], [8], [9], [10] in recent decades due to the growing understanding of brain function and electrophysiological signals. Among them, steady-state visual evoked potentials (SSVEPs) have shown great potential for use in BCIs due to their stable frequency characteristics [11].

Elicitation of the time- and phase-locked SSVEPs is the key to realizing high-performance SSVEP-BCIs. Most studies present stimuli on a liquid crystal display (LCD) screen or light-emitting diode (LED) array [12]. The average ITR of SSVEP-BCI has achieved 325.33 ± 38.17 bits/min with LCD [13]. Nonetheless, LCD and LED monitors were cumbersome and not practical for real-world settings, which limited the application of BCIs in more scenarios [14]. Additionally, in actual control scenarios, users had to pay attention to objects in real scene and the visual stimuli at the same time [15], [16], [17]. The operational burden will grow if the focus is frequently switched between the computer screen and controlled objects. Some studies captured the surrounding scenes using cameras to synchronously present stimuli and controlled objects on the same screen. Kansaku et al. [18] displayed the real scenario on the computer screen using a camera attached to the robot, along with the visual stimuli being presented to elicit the P300 potentials. Stawicki et al. [19] developed a control system for a mobile robot car based on SSVEP-BCI. They presented the live video streams with visual stimuli superimposed on the same screen. However, these studies still relied on cumbersome monitors for real-time video presentation.

Augmented reality (AR) and mixed reality (MR) technologies are capable of combining the real world with virtual

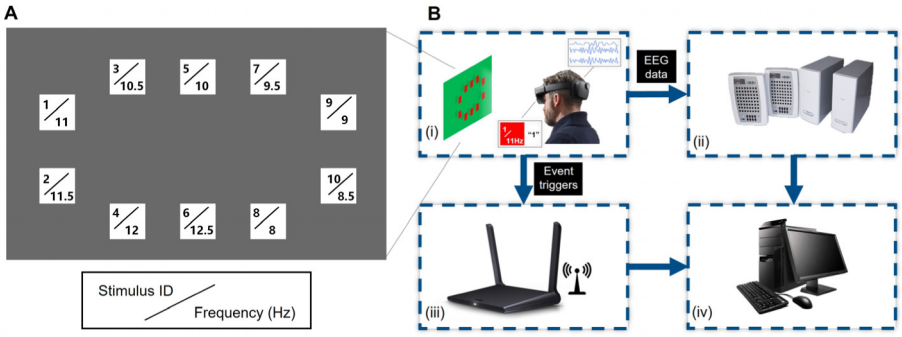

Fig. 1. BCI System based on the Hololens2. (A) Stimulation interface. The stimulus identifiers and flicker frequencies are indicated by numbers on the squares, which are not visible during the experiments. (B) System architecture of the proposed MR-BCI.

information and overlaying virtual graphics onto the real environment. BCI systems can be deployed in AR or MR environments using special head-mounted displays, allowing users to view visual stimuli while still perceiving their external surroundings. In 2011, Takano et al. [20] developed an AR-BCI system for controlling a television and a table lamp. Choi and Jo [21] used SSVEP and motor imagery (MI) as control signals to construct BCIs, successfully controlling a quadcopter with three commands in an AR environment. In 2014, Massari et al. [22] combined BCI and mixed reality (MR) to decode and monitor brain activity.

Color is an important parameter of visual stimulus in BCI systems. SSVEP-BCIs that are deployed in LCD or LED environments have examined how background or stimulus colors affect system performance, but few studies have explored that in MR environments. Bieger et al. [23] studied the effects of multiple stimulus properties on SSVEP responses. The results indicated that multicolor stimuli performed significantly better than solid blue and green stimuli. Tello et al. [24] compared the SSVEP amplitudes elicited by red, blue, and green flickering. They found that the red stimulus evoked greater amplitude which they attributed to higher vigilance. However, Cao et al. [25] reached a different conclusion. They concluded that white visual stimuli activate all three types of optical cones, thereby eliciting the strongest EEG response, as demonstrated by their experiment. Shu et al. [26] found that the more complex the background against which visual stimuli are presented, the worse the SSVEP signal quality. Therefore, improving the performance of BCIs in MR environments is a critical issue, particularly when rendering stimuli in complex backgrounds [27].

This study developed an SSVEP-BCI to explore the interaction between different stimulus colors and backgrounds. The Hololens2, an MR-HMD device, was used as the stimulator. The Hololens2 creates a holographic canvas overlaying the physical environment, offering BCI users a new mode of interaction. Two offline experiments were conducted to optimize the parameters of stimuli presented against various backgrounds. In the first experiment, solid background colors were used to explore the relationship between stimulus colors and background colors. The second experiment was conducted with a colorful background to compare the performance of monochromatic and polychromatic stimuli. Subsequently, an online experiment was conducted to quantitatively assess the system's performance. An improved cross-correlation task-related component analysis based on simulated annealing (SA-xTRCA) algorithm was introduced to calibrate latency jitters across SSVEP trials caused by unstable event trigger transmission [27].

II. Method

A. Experimental Equipment

We developed an SSVEP-BCI in the MR environment. As shown in Fig. 1 (B), the system consisted of four subsystems. Hololens2 was used as the stimulator in this study, which provides an MR environment [28]. EEG data collected by the EEG amplifier were transmitted to a computer, which served as the data processing system. The stimulation program in Hololens2 generated event triggers and sent them to a relay computer via the User Datagram Protocol (UDP), and then connected to the EEG amplifier through the parallel port.

B. Stimulation Design

A 10-command SSVEP stimulus interface was designed and deployed as an application on the Hololens2. The stimulation application was created using Unity 3D and released to Hololens2 via USB. The stimulator device operated at a refresh rate of 60 Hz. Continuous flickering was generated by modulating the RGB values of each visual stimulus using a sinusoidal waveform [29]. The frequencies ranged from 8 to 12.5 Hz with 0.5 Hz intervals. Fig. 1 (A) illustrates the layout of the visual stimuli. Ten squares, each occupying a $6° \times 6°$ field of view, were arranged around the periphery of the interface. Before the flicker started, a yellow '+' visual cue was displayed, instructing subjects to direct their gaze toward the target location. The cue lasted for 1 second. Subsequently, the 10 stimuli flickered simultaneously for a duration of t seconds, where $t = 2$ in the offline experiment. In the online experiment, this duration was adjusted to 1, 1.5, or 2 seconds based on the actual experimental effect for each subject.

C. Experiment Procedure

1) Experiment I: Stimulation Parameter Optimization: In Experiment I, we selected four common colors from everyday environments to create monochromatic backgrounds, while using red and white, which are commonly employed as

TABLE I
RGB VALUES OF STIMULUS AND BACKGROUND COLORS IN EXPERIMENT I

	Color	Abbreviation	RGB value
Stimulus	Red	r	[255,0,0]
	White	w	[255,255,255]
Background	Green	G	[98,252,67]
	Blue	B	[38,155,196]
	Black	K	[66,67,64]
	White	W	[229,223,222]

stimulus colors in SSVEP-BCI systems. We used Photoshop to calculate the RGB values of monochromatic posters. To address the color discrepancy between the photographed images and the actual posters, we adjusted the saturation settings in Photoshop. This ensured that the photographed colors matched the actual colors. The RGB values for all colors are provided in Table I. In the following, we abbreviate 8 conditions in Experiment I as B-r, B-w, G-r, G-w, K-r, K-w, W-r, W-w, where the first capital letter represents background color and the second lowercase letter represents the stimuli color. controlled the room's brightness by closing the curtains and turning on the lights during the experiments. In the experiment, subjects sat 1 meter from the wall, on which a poster was hung to provide the experimental background, and wore an EEG recording cap and the Hololens2. After the stimulation program started, the flashing squares were projected onto the poster. In Experiment I, each condition consisted of ten blocks, with each block containing ten stimuli presented in random order. For every subject, the eight experimental conditions were conducted randomly to avoid potential sequential effects. Subjects took a few minutes' rest between blocks to avoid visual fatigue. The scenes and procedure of Experiment I are shown in Fig. S1 in the Supplementary Material.

2) Experiment II: Online Performance Evaluation: In Experiment II, the poster was replaced by a colorful one, which included the four background colors from Experiment I. The experimental conditions included the following: a) polychromatic stimuli, where white stimuli and the red stimuli were simultaneously presented; b) red-only stimuli; and c) white-only stimuli. For polychromatic stimuli, we adjusted the stimulus color at different positions to create great contrast with the background.

Each experimental condition consisted of an offline experiment followed by an online experiment. The experimental procedure and stimulus sequence for a single trial in the offline experiment were identical to those in Experiment I. Based on the performance in the offline experiment, the stimulus duration was individually set at 1, 1.5, or 2 seconds for each subject in the online experiment. The EEG data collected in the offline experiment were used to compute spatial filters and personalized calibration templates, which were directly applied in the online data analysis. The online experiment involved a cue-guided target task and was structured into three separate blocks. A short beep was produced by the computer after an SSVEP signal was identified to provide feedback on the classification result. The experimental scenes and procedure of Experiment II are shown in Fig. S2 of the Supplementary Material.

D. Participants

Ten healthy subjects (5 males and 5 females, aged 23-26) with normal or corrected-to-normal vision were recruited for both Experiment I and Experiment II. All subjects passed the colorblind test. They were fully informed about the experimental procedure and any possible scenarios that could arise during and after the experiment. The experimental procedure and informed consent forms were approved by the Institutional Review Board at Tianjin University.

E. EEG Acquisition and Data Pre-Processing

EEG data were acquired using a Neuroscan Synamps2 system with 21 electrodes (P7, P5, P3, P1, PZ, P2, P4, P6, P8, PO7, PO5, PO3, POZ, PO4, PO6, PO8, OZ, O1, O2, CB1, CB2) according to the international 10/20 system. The sampling rate of the acquisition device was 1000 Hz. The reference electrode was placed on the top of the head near CZ, and the ground electrode was put on the prefrontal lobe. The EEG signals were bandpass filtered between 0.1 Hz and 100 Hz, and notch-filtered at 50 Hz. During preprocessing, the raw data were first down-sampled to 250 Hz and segmented into EEG epochs according to specific time windows. Then the EEG epochs were bandpass-filtered between 6 Hz and 30 Hz.

F. Classification Algorithm

This study proposed an alignment and classification method for SSVEP, called SA-xTRCA, and compared its performance with four other common algorithms: filter bank canonical correlation analysis (FBCCA) [30], extend canonical correlation analysis (Extend-CCA) [31], task-related component analysis (TRCA) [13], and xTRCA [32].

1) FBCCA: The main idea of FBCCA is to construct multiple filters with different passbands to perform sub-band decomposition. The fundamental and harmonic frequency components ($\boldsymbol{X}_{SB_n}, n = \{1, 2, \ldots, n\}$) are extracted from the original signals $\boldsymbol{X}$ to form multidimensional EEG features. After feature extraction, FBCCA applies Canonical Correlation Analysis (CCA) to each individual sub-band and

calculates the correlation between $\boldsymbol{X}_{SB_n}$ and a set of reference signals $\boldsymbol{Y}_f$ generated for each SSVEP frequency used in the experiment. By aggregating these correlation coefficients, FBCCA effectively utilizes information from multiple harmonics of SSVEP. Detailed information on FBCCA is available in [30].

2) Extend-CCA: Extend-CCA combines the concepts of individual calibration data and filter banks based on the traditional CCA method. For the $k-th$ target, this method integrates three spatial filters to enhance the SNR of SSVEPs: a). $\boldsymbol{w}_X\left(\boldsymbol{X}\overline{\boldsymbol{\chi}}_k\right)$ between the test set $\boldsymbol{X}$ and the training template $\overline{\boldsymbol{\chi}}_k$, b). $\boldsymbol{w}_X\left(\boldsymbol{X}\boldsymbol{Y}_{f_k}\right)$ between $\boldsymbol{X}$ and sine-cosine reference signal $\boldsymbol{Y}_{f_k}$, c). $\boldsymbol{w}_X\left(\overline{\boldsymbol{\chi}}_k\boldsymbol{Y}_{f_k}\right)$ between $\overline{\boldsymbol{\chi}}_k$ and $\boldsymbol{Y}_{f_k}$. Detailed information on Extend-CCA is available in [31].

3) TRCA: TRCA has been commonly employed in the identification of SSVEPs [33], [34], [35], [36] due to its effectiveness in extracting task-related components (TRC). Supposed the $k-th$ training set is $\boldsymbol{\chi}_k \in R^{N_c\times N_s\times N_t}$, where N_c, N_s, and N_t represents the number of EEG channels, sampling points and trials, respectively. TRCA computes a spatial filter $\boldsymbol{w}$ that maximizes the reproducibility during the task period by solving the following constrained optimization problem:

$$\widehat{\boldsymbol{w}} = \underset{w}{\operatorname{argmax}} \frac{\boldsymbol{w}^T\mathbf{S}\mathbf{w}}{\boldsymbol{w}^T\mathbf{Q}\mathbf{w}}, \tag{1}$$

where the matrix $\boldsymbol{S}$ is the sum of covariance matrixes between the $i-th$ trial $\boldsymbol{\chi}_k^i$ and the $j-th$ trial $\boldsymbol{\chi}_k^j$:

$$\boldsymbol{S} = \sum_{i\neq j}^{N_t} \boldsymbol{\chi}_k^i\left(\boldsymbol{\chi}_k^j\right)^T \in R^{N_c\times N_c}. \tag{2}$$

$\boldsymbol{Q}$ is defined as:

$$\boldsymbol{Q} = \sum_{i,j=1}^{N_t} \boldsymbol{\chi}_k^i\left(\boldsymbol{\chi}_k^j\right)^T \in R^{N_c\times N_c}. \tag{3}$$

According to the generalized Rayleigh quotient, $\boldsymbol{w}$ is obtained as the eigenvector corresponding to the maximum eigenvalue λ of the matrix. The EEG background noise is removed by filtering both the test set and training template using the obtained $\boldsymbol{w}$. After that, CCA is employed to compute the correlation value for target recognition. Detailed information on TRCA is available in [13].

4) xTRCA: In our previous study [37], xTRCA was used for SSVEP trial alignment and detection accuracy improvement. Based on TRCA, xTRCA shifted the time window of each signal trial to extract the TRC. The feature value, which indicates the reproducibility across trials, was calculated as an objective function. Trial-to-trial jitter was compensated by optimizing the start time (latency) of the time window.

The initial latencies of a set of trials $\boldsymbol{\chi}_k \in R^{N_c\times N_s\times N_t}$ can form a vector $\boldsymbol{t}_0 = [\tau_0^1,\ldots,\tau_0^i,\ldots,\tau_0^{N_t}]^{\mathrm{T}}$, where τ_0^i is the assumed initial latency for $\boldsymbol{\chi}_k^i$. We can copy the $i-th$ trial $(\boldsymbol{\chi}_k^i)_{\tau_0^i}$ by τ_0^i+1 to $\tau_0^i+N_s$, where N_s is set to 500 (i.e., the length of a trial is 2 second). Following TRCA, we can solve the optimization problem in Equation (1) to obtain the initial spatial filter $\widehat{\boldsymbol{w}}_{\boldsymbol{0}}$. Let $n=1$, $\widehat{\boldsymbol{w}}_{n-1}=\widehat{w}_0$,and $\boldsymbol{t}_{n-1}=\boldsymbol{t}_0$, where n represents the $n-th$ iteration. For trial i from 1 to N_t, we can optimize the τ_{n-1}^i to τ_{n}^i by sliding a window over the $i-th$ trial within the range $[\tau_0^i-\Delta t/2,\ \tau_0^i+\Delta t/2]$ as follows:

$$\tau_n^i = \underset{\boldsymbol{t}_{n-1}}{\operatorname{argmax}}\ \widehat{\boldsymbol{w}}_{n-1}^T\boldsymbol{S}\left((\boldsymbol{X}_k)_{\boldsymbol{t}_{n-1}}\right)\widehat{\boldsymbol{w}}_{n-1}, \tag{4}$$

where Δt is a search range for optimizing trial timings, which has been set to 50. The cross-correlation coefficient between $(\boldsymbol{\chi}_k^i)_{\tau_{n-1}^i}$ and other trials is calculated to identify a new time window that maximizes correlation, thereby reducing inter-trial jitter and converging towards the optimization objective. If the new time window results in an increased eigenvalue λ_n, which represents the trial reproducibility, the time vector timing vector $\boldsymbol{t}_{n-1}$ is subsequently updated:

$$\boldsymbol{t}_{n-1} = [\tau_{n-1}^1,\ldots,\tau_n^i,\ldots,\tau_{n-1}^{N_t}]^{\mathrm{T}}. \tag{5}$$

In accordance with the updated $\mathbf{t}_{n-1}$, $\widehat{w}_{n-1}$ can be recalculated. After iterating through each element in $\mathbf{t}_{n-1}$, the updated timing vector can be obtained as follows:

$$\boldsymbol{t}_n = [\tau_n^1,\ldots,\tau_n^j,\ldots,\tau_n^{N_t}]^{\mathrm{T}}. \tag{6}$$

$\widehat{\boldsymbol{w}}_n$ and $\boldsymbol{t}_n$ will be iterated repeatedly until the λ_n satisfies the convergence condition:

$$\frac{\|\lambda_{n-1}-\lambda_n\|}{\|\lambda_n\|} < \varepsilon, \tag{7}$$

where ε is set to 10^{-4} according to [32], and detailed information on xTRCA is available in [32].

5) SA-xTRCA: The results in [32] and [37] have demonstrated the effectiveness of xTRCA in enhancing reproducibility across multiple SSVEP trials. However, the performance was limited by the iterative process of time vector optimization. Specifically, the time vector obtained by xTRCA may not always represent the global optimum, which can lead to low classification accuracy. In this study, the simulated annealing (SA) method was incorporated to address the local optimum issue in xTRCA.

SA is a probability-based optimization algorithm inspired by the process of solid annealing [38]. Suppose an initial solution x, and an initial system temperature T_0 represent the initial system state. A new solution x' is generated from the neighborhood of x. Let the cost function be $f(x)$, if $f\left(x'\right) < f(x)$, indicating a lower cost, the new solution x' is accepted. If $f\left(x'\right) > f(x)$, the gradient descent algorithm would reject the new solution x'. However, in SA, x' is accept with a probability P, which follows a Boltzmann distribution, as given by Equation (8):

$$P = e^{-\frac{f\left(x'\right)-f(x)}{T}}. \tag{8}$$

Then the system temperature would reduce:

$$T = r\times T, \tag{9}$$

where r is the annealing speed, which means the probability P will decrease with annealing. The system temperature is lowered after several iterations. When P approaches zero, the algorithm converges.

The SA-xTRCA algorithm consists of two parts: (i) Latency calibration for training set and (ii) Classification for test set

(See Fig. S3 in Supplementary Material). In this study, $\mathbf{t}_n$ is the goal of optimization, and the cost function is defined as:

$$f(\boldsymbol{t}_n) = -\lambda_n. \tag{10}$$

P is defined as:

$$P = e^{1/T^{(\lambda_{n-1}-\lambda_n)}}. \tag{11}$$

Specifically, if $\lambda_{n-1} \geq \lambda_n$, a perturbation $\boldsymbol{\mu}$ will be applied to the timing vector $\mathbf{t}_n$ with probability P:

$$\boldsymbol{t}_n = \boldsymbol{t}_n + \boldsymbol{\mu}, \tag{12}$$

and then, the system temperature is reduced. $\boldsymbol{\mu}$ is a vector composed of random integers that perturbs $\mathbf{t}_n$ to move it away from the local optimum. The training set $\boldsymbol{\chi}_k$ is input into part (i) and the calibrated data $(\widehat{\boldsymbol{\chi}}_k)_{\boldsymbol{t}_n}$ along with the spatial filter $\widehat{w}_n$ are output, where $(\widehat{\boldsymbol{\chi}}_k)_{\boldsymbol{t}_n}$ indicates the $k-th$ training trials that were intercepted according to the time vector $\boldsymbol{t}_n$.

Additionally, we developed a classifier to decode multiple-classes SSVEPs. First, the latency of the test trial $\boldsymbol{X}$ is calibrated. N different time windows $\{[t_0+1,\ t_0 + N_s],\ldots,[t_N+1,\ t_N + N_s]\}$ are used to extract multiple epochs$\{(\boldsymbol{X})_{t_1},\ldots,(\boldsymbol{X})_{t_N}\}$, where $t_{\mathrm{m}} = m - \frac{N}{2}, m \in [0, 1, 2, \ldots N]$, and N was set to 50 in this study. The cross-correlation coefficients between the $m-th$ epoch $(\boldsymbol{X})_{t_m}$ and template $(\overline{\boldsymbol{\chi}}_k)_{\boldsymbol{t}_n}$ are calculated:

$$r_m = R((\boldsymbol{X})_{t_m}, (\overline{\boldsymbol{\chi}}_k)_{\boldsymbol{t}_n}, \tag{13}$$

where $R(\cdot\mathrm{E}, \cdot\mathrm{E})$ represents the cross-correlation function. $(\overline{\boldsymbol{\chi}}_k)_{\boldsymbol{t}_n}$ is obtained by averaging over N_t trials:

$$(\overline{\boldsymbol{\chi}}_k)_{\boldsymbol{t}_n} = \frac{1}{N_t}\sum_{i=1}^{N_t}(\boldsymbol{\chi}_k^i)_{\tau_n^i}. \tag{14}$$

The epoch $(\boldsymbol{X})_{t_h}$ that maximized coefficients is selected as the calibrated test data. After spatial filtering, CCA is used to obtain the correlation values between templates and test data as follow:

$$\rho_k = CCA(\widehat{\boldsymbol{w}}_n^T\left(\overline{\boldsymbol{\chi}}_k\right)_{\boldsymbol{t}_n}, \widehat{\boldsymbol{w}}_n^T(\boldsymbol{X})_{t_h}). \tag{15}$$

Index Γ of the target class is determined using the equation below:

$$\Gamma = \underset{k}{\operatorname{argmax}}\,\rho_k. \tag{16}$$

A detailed explanation about SA method is performed in [38].

G. Color Contrast Ratios

Color contrast ratios (CCRs) have been proposed as a measure of the distinctiveness between text and background in web design [39], [40]. In our pervious study, CCRs were induced to evaluate the effect of the interaction between stimulus color and background color on BCI system performance [37]. Suppose two colors C_1 and C_2, with normalized RGB values C_1: $[R_1, G_1, B_1]$ and C_2: $[R_2, G_2, B_2]$, be given. The CCR between C_1 and C_2 is calculated as:

$$CCR = \frac{\max(L_1, L_2) + 0.05}{\min(L_1, L_2) + 0.05}, \tag{17}$$

TABLE II
THE CCRS OF EIGHT EXPERIMENTAL CONDITIONS

Background color	Stimulus color	CCRs	Log (CCRs)
B	r	1.3	0.362
	w	3.2	0.491
G	r	3.0	0.482
	w	1.4	0.146
K	r	2.5	0.146
	w	10.0	0.973
W	r	3.0	0.544
	w	1.3	0.301

where L is defined as

$$L = 0.2126R' + 0.7152G' + 0.0722B', \tag{18}$$

where R' is defined as:

$$R' = \begin{cases} \dfrac{R}{12.92}, & R \leq 0.03928 \\ \left(\dfrac{R+0.055}{1.055}\right)^{2.4}, & R > 0.03928 \end{cases}. \tag{19}$$

G' and B' are calculated in the same way.

To explore the relationship between different color parameters and SSVEP detection accuracy, we calculated CCRs between stimulus colors and background colors. To mitigate the skewness of CCR, a logarithmic transformation was applied. The CCRs and log(CCRs) are listed in Table II.

H. Performance Evaluation

Amplitude and signal-noise-ratio (SNR) have been widely used to evaluate the signal quality of SSVEPs [30], [31], [42]. The SSVEP amplitude at the target frequency, $|y(f)|$, can be obtained using fast Fourier transform (FFT). SNR is defined as the ratio of $|y(f)|$ to the mean amplitude of the four neighboring frequencies on each side:

$$SNR = 20\log_{10}\frac{|y(f)|}{\sum_{k=1}^{4}|y(f-0.5\times k)| + |y(f+0.5\times k)|} \tag{20}$$

The target identification accuracy and ITR were calculated in this study to evaluate BCI system performance. ITR [43] was calculated using the following equation:

$$ITR = \frac{60}{T}\left(\log_2 N_f + P\log_2 P + (1-P)\log_2\frac{1-P}{N_f-1}\right) \tag{21}$$

I. Statistical Analysis

This study employed a variety of statistical methods to analyze the data. A paired t-test was conducted to examine differences in signal amplitude and SNR before and after latency calibration of SSVEP trials using the SA-xTRCA algorithm. The Rayleigh test was applied to assess phase concentration in SSVEP trials before and after calibration. The detail of Rayleigh test will be introduced in the following text. Furthermore, analysis of variance (ANOVA) was utilized to compare classification accuracy across different algorithms

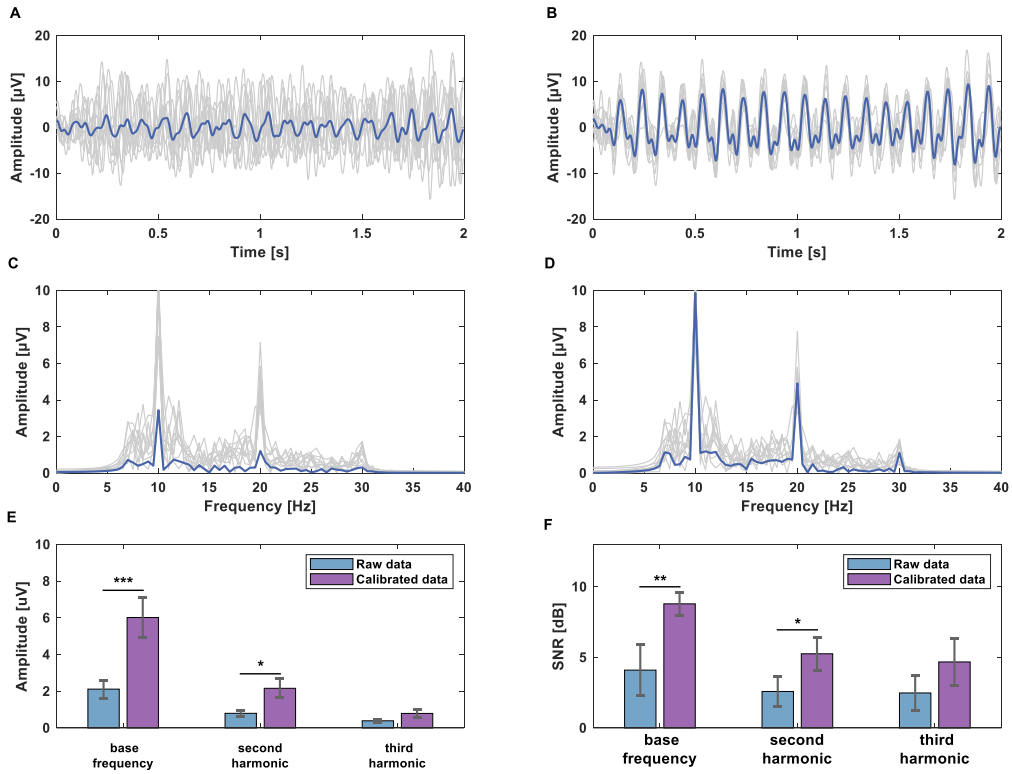

Fig. 2. Performance of SA-xTRCA on latency calibration, using 10 Hz data from Condition K-r. (A) Raw Data Waveform. The gray lines represent individual trials, and the blue line represents the averaging signal. Latency jitters neutralize the TRC, leading to an averaged waveform with diminished amplitude. (B) Calibrated Data Waveform. After calibration, the periodic nature of the averaged waveform is enhanced, showing clearer peaks. (C) Raw Data Spectrum. The blue line represents the spectrum of the averaging signal from (A). The spectrum of the raw data shows less distinct peaks. (D) Calibrated Data Spectrum. The blue line represents the spectrum of the averaged signal from (B). The spectrum of calibrated data exhibits clear peaks at the base frequency, second harmonic, and third harmonic. (E). Amplitude Comparison. (F). SNR Comparison (***$p<0.001$, **$p<0.01$, *$p<0.05$).

and to evaluate BCI performance metrics under various experimental conditions. To address the issue of inflated significance levels due to multiple comparisons, Bonferroni corrections were applied in all analyses involving multiple levels and factors. Statistical analyses were performed using SPSS software (IBM), version 27, and the significance level was set at $p<0.05$.

Rayleigh test is a statistical method commonly used to assess the degree of concentration in directional data [41]. Directional data, such as the SSVEP phase θ_i, can be transformed into a a unit vector on a two-dimensional plane:

$$r_i = (cos\theta_i \quad sin\theta_i)^T. \tag{22}$$

To test whether the phases of multiple SSVEP trials are uniformly distributed over $[0, 2\pi]$ or concentrated in a common direction, the following hypotheses are formulated:

H_0 : The phases are uniformly distributed over $[0, 2\pi]$.

H_A : The phases are not uniformly distributed over $[0, 2\pi]$.

The p-value is computed as follows:

$$P = \exp\left[\sqrt{1 + 4N_t + 4\left(N_t^2 - R_n^2\right)} - (1 + 2N_t)\right], \tag{23}$$

where R_n is defined as:

$$R_n = N_t R, \tag{24}$$

$$R = \left\| \frac{1}{N_t} \sum_i^1 r_i \right\|, \tag{25}$$

III. Result

A. Feature Analysis

This study investigated the characteristics of SSVEP induced by Hololens2, using data from Subject 7 as an illustrative example. As shown in Fig. 2 (A) to (D), latency calibration aligned the trials, enhanced the periodic nature of the averaged waveforms, and increased the amplitudes at the target frequency. Fig. 2 (E) and (F) show the improvements in amplitudes and SNRs after calibration. Paired t-tests were performed and indicated significant differences in both amplitudes and SNRs at the fundamental (amplitude: $p<0.001$***; SNR: $p<0.01$**) and second harmonic frequencies (amplitude: $p<0.05$*; SNR: $p<0.05$*). We also calculated and averaged the SSVEP amplitudes and SNRs across all conditions and frequencies. The results indicated that the amplitudes of the fundamental, second, and third harmonics improved by 2.83, 1.47, and 0.25 μ V, respectively, following calibration. Similarly, post-SNR improvements of 3.42, 3.42, and 1.97 dB were observed for the respective harmonics.

In addition, we calculated the phase of each trial before and after calibration, and plotted them on a unit circle (Fig. 3). The blue circles are more clustered than the red ones, indicating that the phase difference across calibrated trials was smaller. The Rayleigh test was used to assess the degree of phase concentration. The resultant vector length and p-value of Rayleigh test across 10 subjects before and after latency calibration are shown in the form of dumbbell plots, as illustrated in Fig. 4.

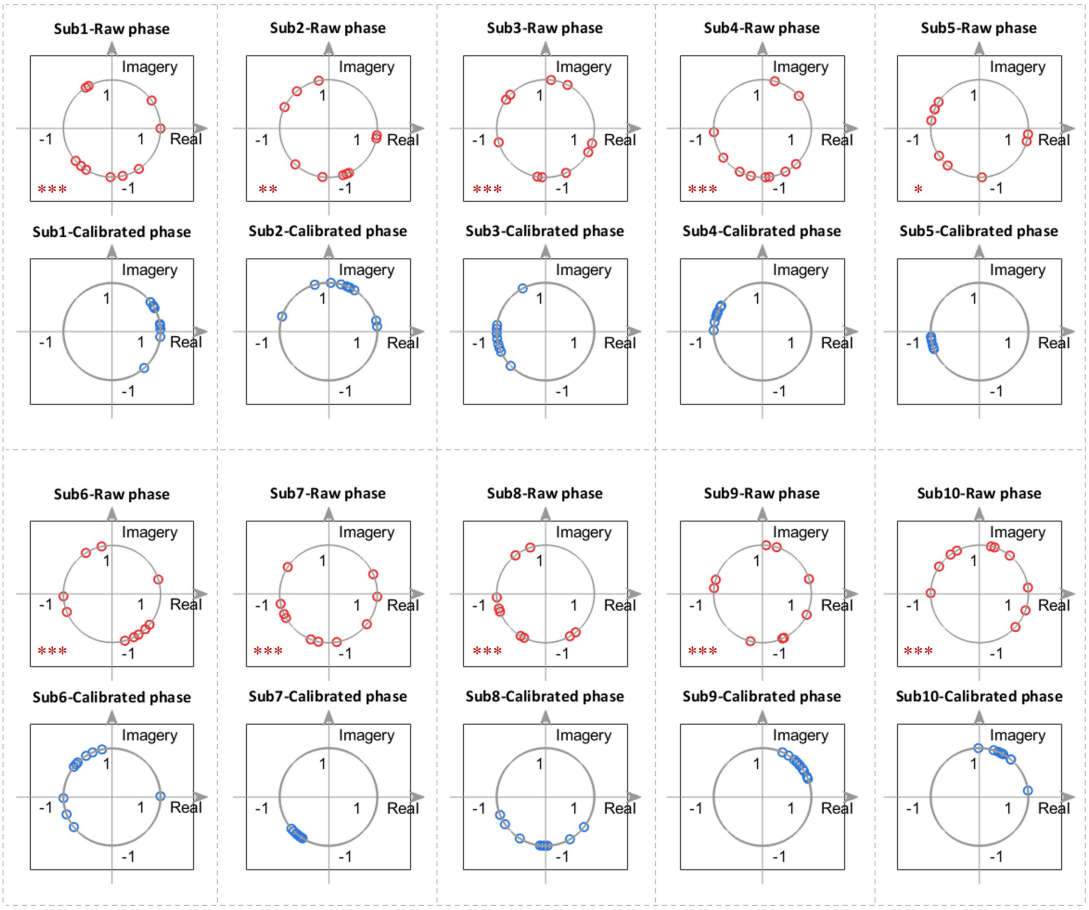

Fig. 3. The phase distribution diagrams of raw and calibrated data at 10 Hz for all ten subjects. The red circles indicate the phases of raw data, while the blue circles indicate the phases of calibrated trials. The asterisk annotations in the subplots indicate the significance level of phase concentration. (*p<0.05, **p<0.01, ***p<0.001).

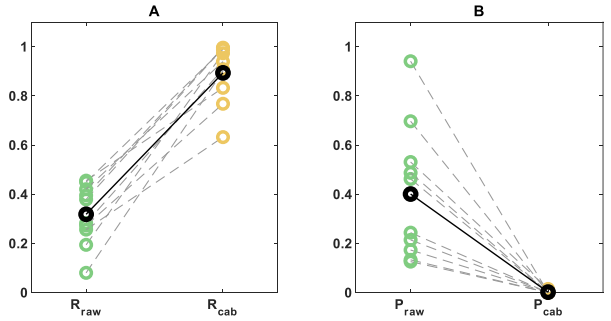

Fig. 4. The resultant vector length and p-value of Rayleigh test across 10 subjects before and after latency calibration. R_{raw} represent the resultant vector length of raw data, and R_{cab} represent the resultant vector length of calibrated data. p_{raw} represent the p-values of raw data, and p_{cab} represent the p-value of calibrated data.

The results indicated that, prior to calibration, the p-values for all subjects were greater than 0.05, while after calibration, the p-values for all subjects were less than 0.05. This indicates that the phases were more concentrated in the same direction after calibration. The p-values are annotated with asterisks (*) in each subplot.

B. Target Identification Performance

To verify the classification performance of the SA-xTRCA algorithm, we compared its effectiveness against five other algorithms. Fig. 5 shows the average accuracies across all subjects with different data lengths from 1s to 2s in an interval of 0.1s. The comparison results indicated that the SA-xTRCA algorithm consistently achieved the highest performance across all data lengths, and xTRCA was outperformed than other three algorithms. Notably, TRCA performed only slightly better than random accuracy, despite being regarded as the optimal algorithm in many previous studies. For uncalibrated data, feature analysis revealed that the characteristics from multiple trials might cancel each other out when averaged due to latency jitters. As a result, the correlation between the averaged template signal and the test trial was diminished. In contrast, sine and cosine signals, which match the target frequencies, exhibited more stable frequency characteristics. Consequently, FBCCA and Extend-CCA, which use these sine-cosine signals as training templates, outperformed TRCA. A more detailed explanation of the failure of the TRCA algorithm is provided in Section B of the Supplementary Material.

Two-way repeated measures ANOVAs (algorithm × data length) were conducted to assess accuracy, revealing significant main effects for both algorithm ($F(4,36) = 1692.26$, $p<0.001^*$*) and data length ($F(10,90) = 3.19$, $p<0.01^*$*). However, no significant interaction was found between these two factors ($F(40,360) = 1.12$, $p>0.05$). Pairwise comparisons

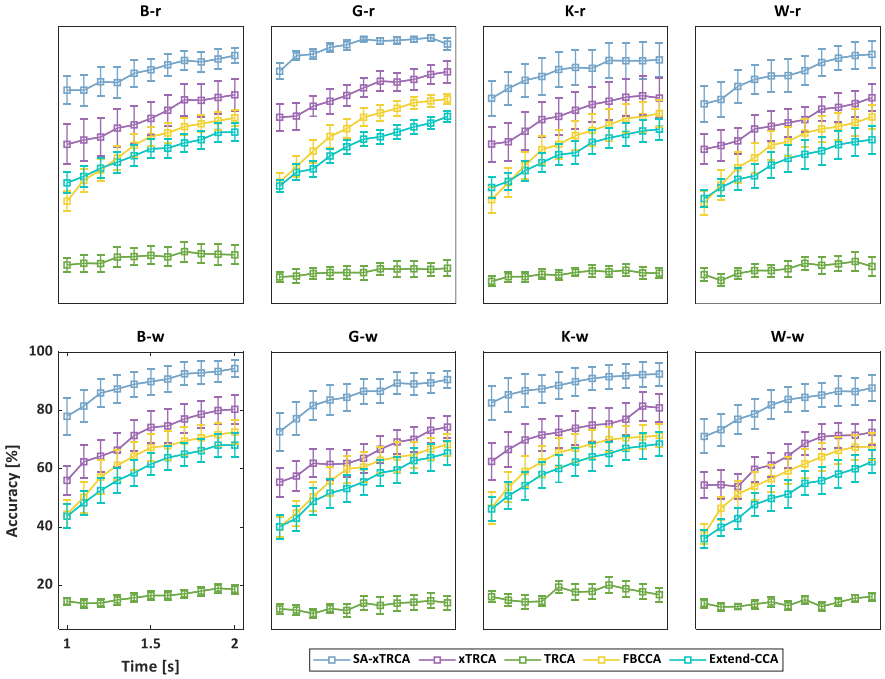

Fig. 5. Performance comparison of five algorithms using the recorded data from the eight experimental conditions.

showed that the SA-xTRCA algorithm significantly outperformed all other methods ($p<0.001^{**}$).

C. Computational Time of the SA-xTRCA

We calculated the time required for the proposed algorithm to train calibrated templates and perform classification. The dataset included data from all experimental conditions of 10 subjects in Experiment I, and classification was carried out using 10-fold cross-validation. The latency calibration and spatial filter construction time for a single class template was denoted as t_{train}, while the latency calibration and pattern recognition time for a single test trial was denoted as t_{test}. The results showed that the average values of t_{train} and t_{test} were 274.52 ms ± 296.20 ms and 12.31 ms ± 0.31 ms, respectively. The maximum values were 451.23 ms and 19.76 ms, respectively. For comparison, the average time required by TRCA method for the same dataset were 48.53 ms ± 32.48 ms for t_{train} and 9.33 ms ± 0.31 ms for t_{test}. Although the proposed algorithm requires more time for templates construction, this step can be completed during the preparation phase before online experiments. The classification time for test trial still meets the real-time requirements of an online task.

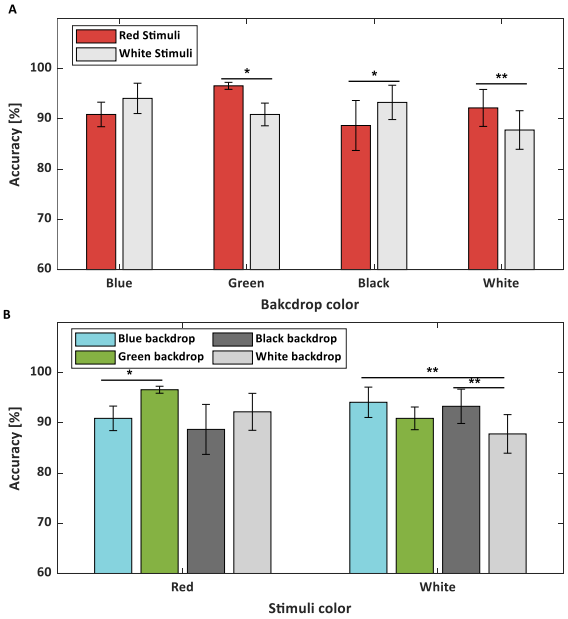

Fig. 6. The average accuracies across 10 subjects. (A) Differential accuracies between stimulus colors with the same background ($^{**}p<0.01$, $^{*}p<0.05$); (B) Differential accuracies among background colors with the same stimuli ($^{**}p<0.01$, $^{*}p<0.05$).

D. Parameter Optimization

In Experiment I, we calculated the SSVEP detection accuracies under different stimuli and background color conditions, as shown in Fig. 6. Specifically, the accuracies were as follows: 90.90 ± 2.44% for B-r, 96.60 ± 0.70% for G-r, 88.70 ± 4.98% for K-r, 92.20 ± 3.68% for W-r, 94.10 ± 3.02% for B-w, 90.90 ± 2.26% for G-w, 93.30 ± 3.42% for K-w, 87.80 ± 3.84% for W-w. Based on these results, we can conclude that the stimulus color yielding the highest detection accuracy for each background color is as follows: red for green and blue backgrounds, white for black and white backgrounds, and red for both green and black backgrounds.

A two-way repeated measures ANOVA (stimuli colors × background colors) was conducted to analyze accuracy. The results revealed a significant interaction effect between the two factors ($F(3,21) = 7.507$; $p<0.01^{**}$). As shown in Fig. 6 (A), paired t-tests show that red stimuli significantly outperformed on the green ($p<0.05^{*}$) and white ($p<0.05^{**}$) background, while white stimuli achieved better performance on the blue and black backgrounds ($p<0.05^{*}$). Fig. 6 (B) indicates that

TABLE III
ACCURACY AND ITR OF ONLINE EXPERIMENTS

Subject	Stimulus time [s]	Accuracy [%]			ITR [bits/min]		
		polychrome	red	white	polychrome	red	white
1	1	80.00	63.00	70.00	58.98	35.95	44.69
2	1.5	100.00	83.00	93.00	79.73	51.01	65.62
3	1	87.00	74.00	67.00	70.57	50.13	40.83
4	2	90.00	83.00	67.00	50.72	42.51	27.22
5	2	70.00	63.00	60.00	29.79	23.97	21.66
6	1	93.00	77.00	87.00	82.02	54.45	70.57
7	2	93.33	86.67	70.00	55.14	46.66	29.79
8	1.5	93.00	73.00	97.00	65.62	38.99	72.78
9	2	90.00	65.00	40.00	50.72	25.57	8.98
10	2	73.00	76.00	60.00	32.49	35.32	21.66
Ave	-	**86.93**	74.37	71.10	**57.58**	40.45	40.38
Std	-	2.89	2.57	5.15	5.31	3.14	6.77

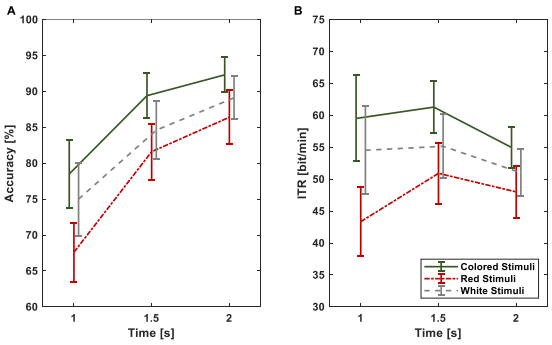

Fig. 7. The average accuracy (A) and ITR (B) of the 3 experimental conditions across 10 subjects in offline experiment of Experiment II.

green background was significantly more suitable than blue background ($p<0.05^*$) for red stimuli, while blue background ($p<0.01^*$) and black background($p<0.01^*$) were significantly more suitable than the white background for white stimuli.

E. System Performance

Fig. 7 (A) and (B) show the accuracies and ITRs for three experimental conditions with data lengths of 1s, 1.5s, and 2s during the offline stage. The average accuracies across all subjects indicated that polychromatic stimuli outperformed monochromatic stimuli for all data lengths. The highest average ITR were 61.209 ± 4.11 bits/min for polychromatic stimuli, 50.91 ± 4.75 bits/min for red stimuli, and 55.15 ± 5.04 bits/min for white stimuli, all with a 1.5s data length.

Two-way repeated measure ANOVAs (stimuli colors × data length) were conducted both on accuracy and ITR. The results revealed significant main effect of stimuli color (accuracy: $F(2,18) = 6.243$, $p<0.05^*$; ITR: $F(2,18) = 8.804$, $p<0.01^*$) and data length (accuracy: $F(2,22) = 44.101$, $p<0.001^{**}$; ITR: $F(2,18) = 12.260$, $p<0.01^*$). Specifically, polychromatic stimuli significantly outperformed red stimuli across all data lengths, while only significantly outperformed white stimuli using data with a 1.5s data length.

After acquiring offline data, the online task was immediately conducted with one polychromatic stimulus and two monochromatic stimuli. The stimulus duration in the online experiment was individually optimized based on the highest ITR calculated in offline experiment. The classification accuracies and ITRs were listed in Table III. For polychromatic stimuli, the average ITR in online experiment was 57.58 bits/min and the peak ITR of 82.02 bits/min achieved by subject 6. For red and white stimuli, the highest ITR was 54.45bits/min and 72.78 bits/min, respectively. The results indicated that most of subjects performed better with the polychromatic stimuli in online task.

IV. DISCUSSION

Extending application scope and enhancing system interactivity are critical issues for the further development of BCI [44]. Presenting visual stimuli in an MR environment is a feasible way to achieve seamless interaction between the BCI and surrounding environment within the same vision field. This approach also provides a more portable and flexible way to implant BCIs into real-world scenarios. In this study, we developed an SSVEP-based MR-BCI and evaluated its performance under various stimulus and background color conditions.

We initially conducted a qualitative analysis to investigate the relationship between stimulus background colors and SSVEP detection accuracy in Experiment I. Following this, a quantitative metric was introduced to model this relationship. The results from Experiment I indicated that the accuracy of target recognition was significantly influenced by the color combinations of the stimuli and their backgrounds. Red stimuli were most effectively presented against lighter backgrounds, such as green or white, while white stimuli performed better against darker backgrounds, such as black or blue. One plausible explanation for these findings is that the evoked SSVEP signals become more pronounced when there is greater color contrast between the stimulus and its background. In 2012, Conway et al. [45] investigated the role of specific neurons in macaque V1 in color contrast, and found that these cells responded more strongly to red and green sequences or to adjacent red/green stimuli, demonstrating color opponency. This phenomenon involves an excitatory response to one color and an inhibitory response to its opposing color. To explore the mapping relationship between different color combinations and accuracy, we used color contrast ratios (CCRs). The results from Experiment I demonstrated a potential non-linear relation between CCR and accuracy. Similar findings have been reported in other studies [4], [5], [6], [7]. These studies showed

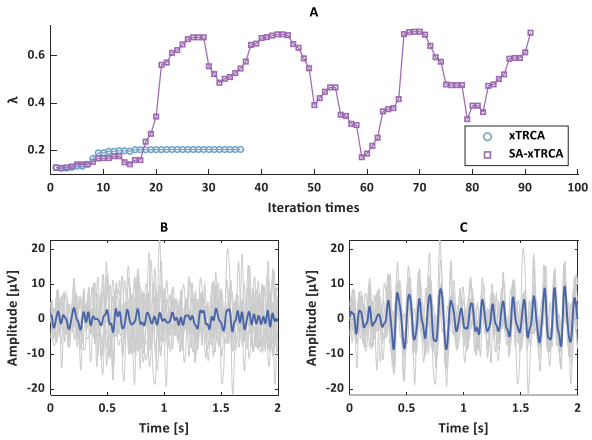

Fig. 8. Performance comparison between xTRCA and SA-xTRCA. (A) Trends in the objective function, λ, during the iterations of xTRCA and SA-xTRCA. (B) The waveform of calibrated data obtained with xTRCA. The grey lines represent individual trials, and the blue line represents the averaging signal. (C) The waveform of calibrated data obtained with SA-xTRCA. The calibrated data using SA-xTRCA show a marked reduction in latency discrepancies across trials and an enhanced prominence of frequency characteristics in the averaged signal.

that at lower contrast levels, the amplitude of VEPs increased rapidly with contrast, but as contrast continued to rise, the rate of amplitude increase slowed. Nevertheless, we observed that K-w is an outlier as it had the highest CCR but lower accuracy compared to G-r and B-w. Many studies have reported that white stimuli on a black background tend to achieve the highest performance when using PC screens [22], [23], [24], [46], [47]. We speculate that the discrepancy in our results may be due to the high contrast of stimuli presented on the Hololens2, which could lead to visual fatigue. Mouli et al. [48] found that the FFT amplitude of SSVEP increased with luminance but declined at the maximum luminance. Additionally, several studies have suggested that the evoked response to luminance or color contrast is nonlinear [45], [49], [50]. Future research should explore a wider range of color combinations for stimuli and backgrounds to better map the relationship between CCR and system performance. Specifically, there may be a critical point beyond which increasing CCR could lead to a sharp decline in BCI performance. By identifying and adjusting stimulus color to optimize CCR against the background, the separability of the evoked SSVEP signals can be enhanced.

During the experiment, we observed latency jitters across trials, which were caused by unstable transmission of event triggers from the stimulation devices to the amplifier. The jitters reduced the reproducibility across trials, leading to poor performance in classification methods that relied on individual templates. Because averaging unaligned trials would weaken the signal features. This study proposed the SA-xTRCA algorithm, which calibrates and aligns the latency of each SSVEP trial based on the TRC. Unlike traditional gradient descent algorithm, which accepted only iteration that minimize the cost function, SA occasionally allows uphill steps to search for the global optimum [51]. As a classical stochastic searching optimization algorithm, SA have been used in previous studies to optimize the model parameters or classification algorithms, resulting improved performance [52], [53], [54]. The SA-xTRCA achieved a significantly higher classification accuracy than xTRCA, as shown in Fig. 5. Fig. 8 (A) shows the variation of λ throughout the iterations for both xTRCA and SA-xTRCA. Compared to xTRCA, SA-xTRCA consistently achieved higher λ values after each iteration, despite requiring more iteration rounds. The waveforms of the calibrated trials obtained by xTRCA and SA-xTRCA are shown in Fig. 8 (B) and (C), respectively. These results suggest that incorporation the SA method can effectively prevent convergence to a local optimum. The decoding efficiency of traditional algorithms heavily depend on precisely calibrated triggers at the onset of each trial. However, ensuring that each trigger remains undisturbed during transmission is challenging when implementing BCI systems in real-world settings. To address this issue, this study provided an effective method for preventing triggers misalignment.

V. Conclusion

In this study, an SSVEP-BCI was developed using an MR device and the impact of stimulus and background color interactions on SSVEP detection accuracy was explored. The SA-xTRCA algorithm was proposed to address latency jitters across trials, significantly improving performance. Our results showed that red stimuli performed best against green and white backgrounds, while white stimuli were more effective on black and white backgrounds. The polychromatic stimulus outperformed monochromatic stimuli on colorful backgrounds. A potential nonlinear positive correlation between SSVEP detection accuracy and CCRs was observed, emphasizing the importance of color contrast. This study demonstrated an effective approach to enhance SSVEP signal characteristics and highlighted the need for optimizing stimulus-color combinations to improve BCI performance in MR environments.

Acknowledgment

The authors sincerely thank all subjects for their participation.

References

[1] J. R. Wolpaw, "Brain–computer interfaces as new brain output pathways," *J. Physiol.*, vol. 579, no. 3, pp. 613–619, Mar. 2007.

[2] M. Xu, X. Xiao, Y. Wang, H. Qi, T.-P. Jung, and D. Ming, "A brain–computer interface based on miniature-event-related potentials induced by very small lateral visual stimuli," *IEEE Trans. Biomed. Eng.*, vol. 65, no. 5, pp. 1166–1175, May 2018.

[3] Y. Dong, S. Wang, Q. Huang, R. W. Berg, G. Li, and J. He, "Neural decoding for intracortical brain–computer interfaces," *Cyborg Bionic Syst.*, vol. 4, p. 44, Jan. 2023.

[4] C. Guger, H. Ramoser, and G. Pfurtscheller, "Real-time EEG analysis with subject-specific spatial patterns for a brain–computer interface (BCI)," *IEEE Trans. Rehabil. Eng.*, vol. 8, no. 4, pp. 447–456, Dec. 2000.

[5] J. A. Wilson, E. A. Felton, P. C. Garell, G. Schalk, and J. C. Williams, "ECoG factors underlying multimodal control of a brain–computer interface," *IEEE Trans. Neural Syst. Rehabil. Eng.*, vol. 14, no. 2, pp. 246–250, Jun. 2006.

[6] C. Reichert, S. Dürschmid, H.-J. Heinze, and H. Hinrichs, "A comparative study on the detection of covert attention in event-related EEG and MEG signals to control a BCI," *Frontiers Neurosci.*, vol. 11, Oct. 2017, Art. no. 299495.

[7] Y. Pei et al., "A tensor-based frequency features combination method for brain–computer interfaces," *IEEE Trans. Neural Syst. Rehabil. Eng.*, vol. 30, pp. 465–475, 2022.

[8] X. Zhou, M. Xu, X. Xiao, Y. Wang, T.-P. Jung, and D. Ming, "Detection of fixation points using a small visual landmark for brain–computer interfaces," *J. Neural Eng.*, vol. 18, no. 4, Aug. 2021, Art. no. 046098.

[9] J. Han, M. Xu, X. Xiao, W. Yi, T.-P. Jung, and D. Ming, "A high-speed hybrid brain–computer interface with more than 200 targets," *J. Neural Eng.*, vol. 20, no. 1, Feb. 2023, Art. no. 016025.

[10] X. Xiao et al., "Enhancement for P300-speller classification using multi-window discriminative canonical pattern matching," *J. Neural Eng.*, vol. 18, no. 4, Aug. 2021, Art. no. 046079.

[11] Y. Wang, X. Gao, B. Hong, C. Jia, and S. Gao, "Brain–computer interfaces based on visual evoked potentials," *IEEE Eng. Med. Biol. Mag.*, vol. 27, no. 5, pp. 64–71, Sep. 2008.

[12] Z. Wu, Y. Lai, Y. Xia, D. Wu, and D. Yao, "Stimulator selection in SSVEP-based BCI," *Med. Eng. Phys.*, vol. 30, no. 8, pp. 1079–1088, Oct. 2008.

[13] M. Nakanishi, Y. Wang, X. Chen, Y.-T. Wang, X. Gao, and T.-P. Jung, "Enhancing detection of SSVEPs for a high-speed brain speller using task-related component analysis," *IEEE Trans. Biomed. Eng.*, vol. 65, no. 1, pp. 104–112, Jan. 2018.

[14] J. Zhang, J. Li, Z. Huang, D. Huang, H. Yu, and Z. Li, "Recent progress in wearable brain–computer interface (BCI) devices based on electroencephalogram (EEG) for medical applications: A review," *Health Data Sci.*, vol. 3, Jan. 2023, Art. no. 0096.

[15] X. Chen, B. Zhao, Y. Wang, and X. Gao, "Combination of high-frequency SSVEP-based BCI and computer vision for controlling a robotic arm," *J. Neural Eng.*, vol. 16, no. 2, Apr. 2019, Art. no. 026012.

[16] K. LaFleur, K. Cassady, A. Doud, K. Shades, E. Rogin, and B. He, "Quadcopter control in three-dimensional space using a noninvasive motor imagery-based brain–computer interface," *J. Neural Eng.*, vol. 10, no. 4, Aug. 2013, Art. no. 046003.

[17] J. Long, Y. Li, H. Wang, T. Yu, J. Pan, and F. Li, "A hybrid brain computer interface to control the direction and speed of a simulated or real wheelchair," *IEEE Trans. Neural Syst. Rehabil. Eng.*, vol. 20, no. 5, pp. 720–729, Sep. 2012.

[18] K. Kansaku, N. Hata, and K. Takano, "My thoughts through a robot's eyes: An augmented reality-brain–machine interface," *Neurosci. Res.*, vol. 66, no. 2, pp. 219–222, Feb. 2010.

[19] P. Stawicki, F. Gembler, and I. Volosyak, "Driving a semiautonomous mobile robotic car controlled by an SSVEP-based BCI," *Comput. Intell. Neurosci.*, vol. 2016, pp. 1–14, Jan. 2016.

[20] K. Takano, N. Hata, and K. Kansaku, "Towards intelligent environments: An augmented reality–brain–machine interface operated with a see-through head-mount display," *Frontiers Neurosci.*, vol. 5, Sep. 2011, Art. no. 8448.

[21] J. Choi and S. Jo, "Application of hybrid brain–computer interface with augmented reality on quadcopter control," in *Proc. 8th Int. Winter Conf. Brain-Comput. Interface (BCI)*, Feb. 2020, pp. 1–5.

[22] D. De Massari et al., "Fast mental states decoding in mixed reality," *Frontiers Behav. Neurosci.*, vol. 8, Nov. 2014, Art. no. 415.

[23] J. Bieger, G. G. Molina, and D. Zhu, "Effects of stimulation properties in steady-state visual evoked potential based brain–computer interfaces," in *Proc. Annu. Int. Conf. IEEE Eng. Med. Biol. Soc.*, Aug. 2010, pp. 3345–3348.

[24] R. J. M. G. Tello, S. M. T. Müller, A. Ferreira, and T. F. Bastos, "Comparison of the influence of stimuli color on steady-state visual evoked potentials," *Res. Biomed. Eng.*, vol. 31, no. 3, pp. 218–231, Sep. 2015.

[25] T. Cao, F. Wan, P. U. Mak, P.-I. Mak, M. I. Vai, and Y. Hu, "Flashing color on the performance of SSVEP-based brain–computer interfaces," in *Proc. Annu. Int. Conf. IEEE Eng. Med. Biol. Soc.*, Aug. 2012, pp. 1819–1822.

[26] X. Shu, L. Yao, J. Meng, X. Sheng, and X. Zhu, "Visual stimulus background effects on SSVEP-based brain–computer interface," in *Proc. 6th Int. Conf. Intell. Robot. Appl.*, Jan. 2013, pp. 453–462.

[27] Y. Ke, P. Liu, X. An, X. Song, and D. Ming, "An online SSVEP-BCI system in an optical see-through augmented reality environment," *J. Neural Eng.*, vol. 17, no. 1, Feb. 2020, Art. no. 016066.

[28] X. Wang, S. Guo, Z. Xu, Z. Zhang, Z. Sun, and Y. Xu, "A robotic teleoperation system enhanced by augmented reality for natural human–robot interaction," *Cyborg Bionic Syst.*, vol. 5, Jan. 2024, Art. no. 0098.

[29] Y. Wang and T.-P. Jung, "Visual stimulus design for high-rate SSVEP BCI," *Electron. Lett.*, vol. 46, no. 15, pp. 1057–1058, 2010.

[30] X. Chen, Y. Wang, S. Gao, T.-P. Jung, and X. Gao, "Filter bank canonical correlation analysis for implementing a high-speed SSVEP-based brain–computer interface," *J. Neural Eng.*, vol. 12, no. 4, Aug. 2015, Art. no. 046008.

[31] X. Chen, Y. Wang, M. Nakanishi, X. Gao, T.-P. Jung, and S. Gao, "High-speed spelling with a noninvasive brain–computer interface," *Proc. Nat. Acad. Sci. USA*, vol. 112, no. 44, pp. E6058–E6067, Nov. 2015.

[32] H. Tanaka and M. Miyakoshi, "Cross-correlation task-related component analysis (xTRCA) for enhancing evoked and induced responses of event-related potentials," *NeuroImage*, vol. 197, pp. 177–190, Aug. 2019.

[33] J. Mei et al., "Using SSVEP-BCI to continuous control a quadcopter with 4-DOF motions," in *Proc. 42nd Annu. Int. Conf. IEEE Eng. Med. Biol. Soc. (EMBC)*, Jul. 2020, pp. 4745–4748.

[34] K. Lin, X. Chen, X. Huang, Q. Ding, and X. Gao, "A hybrid BCI speller based on the combination of EMG envelopes and SSVEP," *Appl. Informat.*, vol. 2, no. 1, pp. 1–12, Dec. 2015.

[35] Q. Sun, M. Chen, L. Zhang, C. Li, and W. Kang, "Similarity-constrained task-related component analysis for enhancing SSVEP detection," *J. Neural Eng.*, vol. 18, no. 4, Aug. 2021, Art. no. 046080.

[36] J. Tang et al., "A brain–computer interface based on multifocal SSVEPs detected by inter-task-related component analysis," *IEEE Access*, vol. 8, pp. 138539–138550, 2020.

[37] F. He et al., "Optimization of stimulus color for SSVEP-based brain–computer interfaces in mixed reality," in *Proc. Int. Workshop Human Brain Artif. Intell.*, Singapore. Springer, Nov. 2022, pp. 183–191.

[38] A. O. Elnabawy, S. E. K. Fateen, and A. Bonilla-Petriciolet, "Simulated annealing applications in thermodynamic calculations," in *Simulated Annealing: Strategies, Potential Uses and Advantages*, E. Ahmed, F. Seif-Eddeen, and B. P. Adrian, Eds., Commack, NY, USA: Nova, 2014, pp. 139–158.

[39] W. W. W. Consortium, "Web content accessibility guidelines (WCAG) 2.0," World Wide Web Consortium (W3C), Cambridge, MA, USA, Tech. Rep. WCAG 2.0, 2015.

[40] T. Smith and J. Guild, "The C.I.E. Colorimetric standards and their use," *Trans. Opt. Soc.*, vol. 33, no. 3, pp. 73–134, Jan. 1931.

[41] P. Berens, "CircStat: A MATLAB toolbox for circular statistics," *J. Stat. Softw.*, vol. 31, no. 10, pp. 1–21, 2009.

[42] Z. Yao, Y. Wang, C. Yang, W. Pei, X. Gao, and H. Chen, "An online brain–computer interface in mobile virtual reality environments," *Integr. Comput.-Aided Eng.*, vol. 26, no. 4, pp. 345–360, Sep. 2019.

[43] J. R. Wolpaw, N. Birbaumer, D. J. McFarland, G. Pfurtscheller, and T. M. Vaughan, "Brain–computer interfaces for communication and control," *Clin. Neurophysiol.*, vol. 113, no. 6, pp. 767–791, 2002.

[44] M. Xu, F. He, T.-P. Jung, X. Gu, and D. Ming, "Current challenges for the practical application of electroencephalography-based brain–computer interfaces," *Engineering*, vol. 7, no. 12, pp. 1710–1712, Dec. 2021.

[45] B. R. Conway, D. H. Hubel, and M. S. Livingstone, "Color contrast in macaque V1," *Cerebral Cortex*, vol. 12, no. 9, pp. 915–925, Sep. 2002.

[46] X. Duart, E. Quiles, F. Suay, N. Chio, E. García, and F. Morant, "Evaluating the effect of stimuli color and frequency on SSVEP," *Sensors*, vol. 21, no. 1, p. 117, Dec. 2020.

[47] A. Duszyk et al., "Towards an optimization of stimulus parameters for brain–computer interfaces based on steady state visual evoked potentials," *PLoS ONE*, vol. 9, no. 11, Nov. 2014, Art. no. e112099.

[48] S. Mouli and R. Palaniappan, "Eliciting higher SSVEP response from LED visual stimulus with varying luminosity levels," in *Proc. Int. Conf. Students Appl. Eng. (ICSAE)*, Oct. 2016, pp. 201–206.

[49] D. G. Albrecht and D. B. Hamilton, "Striate cortex of monkey and cat: Contrast response function," *J. Neurophysiol.*, vol. 48, no. 1, pp. 217–237, Jul. 1982.

[50] G. S. Souza, B. D. Gomes, C. A. Saito, M. da Silva Filho, and L. C. L. Silveira, "Spatial luminance contrast sensitivity measured with transient VEP: Comparison with psychophysics and evidence of multiple mechanisms," *Investigative Opthalmol. Vis. Sci.*, vol. 48, no. 7, pp. 3396–3404, Jul. 2007.

[51] J. Rudy and D. Żelazny, "Multi-criteria fuel distribution: A case study," in *Proc. 14th Int. Conf. Artif. Intell. Soft Comput. (ICAISC)*, Jan. 2015, pp. 272–281.

[52] S. Kirkpatrick, C. D. Gelatt, and M. P. Vecchi, "Optimization by simulated annealing," *Science*, vol. 220, pp. 671–680, May 1983.

[53] M. Hamedi, Sh-H. Salleh, C. M. Ting, A. B. M. Noor, and I. M. Rezazadeh, "Multiclass self-paced motor imagery temporal features classification using least-square support vector machine," in *Proc. IEEE 19th Int. Funct. Electr. Stimulation Soc. Annu. Conf. (IFESS)*, Sep. 2014, pp. 1–5.

[54] Y. Liu, H. Huang, F. Xiao, R. Malekian, and W. Wang, "Classification and recognition of encrypted EEG data based on neural network," *J. Inf. Secur. Appl.*, vol. 54, Oct. 2020, Art. no. 102567.